

Article

Breast Cancer Detection in Mammography Images: A CNN-Based Approach with Feature Selection

Zahra Jafari ¹, and Ebrahim Karami ^{1,*}

Department of Engineering and Applied Sciences, Memorial University, St. John's, NL, A1B 3X5, Canada, zjafari@mun.ca

* Correspondence: ekarami@mun.ca; Tel.: +1-709-219-1633

Abstract: The prompt and accurate diagnosis of breast lesions, including the distinction between cancer, non-cancer, and suspicious cancer, plays a crucial role in the prognosis of breast cancer. In this paper, we introduce a novel method based on feature extraction and reduction for detection of breast cancer in mammography images. First, we extract features from multiple pre-trained convolutional neural network (CNN) models, and then concatenate them. The most informative features are selected based on their mutual information with the target variable. Subsequently, the selected features can be classified using a machine learning algorithm. We evaluate our approach using four different machine learning algorithms, and our results demonstrate that the neural network-based classifier yields an accuracy as high as 92% for the RSNA dataset which is a new dataset that provides two views and additional features such as age. We compare our proposed algorithm with state-of-the-art methods and demonstrate its superiority, particularly in terms of accuracy and sensitivity. For the MIAS dataset, we achieve an accuracy as high as 94.5%, and for the DDSM dataset, an accuracy of 96% is attained. These results highlight the effectiveness of our method in accurately diagnosing breast lesions and surpassing existing approaches.

Keywords: breast cancer; Convolutional Neural Network (CNN); computer aided diagnosis (CAD); feature selection; feature classification; mammography images

1. Introduction

Breast cancer (BC) is a widespread form of cancer with millions of new diagnoses and deaths each year [1]. In 2020 alone, there were 2.3 million new breast cancer diagnoses and 685,000 deaths [2]. Although mortality rates have declined due to the implementation of regular mammography screening, early detection and treatment remain important for reducing cancer fatalities [3]. Currently, early detection of BC from radiology images requires the expertise of highly trained radiologists. A looming shortage of radiologists in several countries will likely worsen this problem [4]. Mammography screening also leads to a high incidence of false positive results. This can result in unnecessary anxiety, inconvenient follow-up care, extra imaging tests, and sometimes a need for tissue sampling (often a needle biopsy) [5-6]. Additionally, machine learning techniques have the potential to improve the process of evaluating screening mammograms by radiologists [7]. Deep learning as a subset of machine learning in recent years has revolutionized the interpretation of diagnostic imaging studies [8]. A convolutional neural network (CNN) is one of the most significant networks in the deep learning field [9]. Compared to traditional screening techniques, computer aided diagnosis (CAD) systems utilizing convolutional neural networks (CNN) offer faster, more reliable, and more robust screening. CNNs have emerged as a prominent method for pattern recognition in image analysis [10]. CNN has been extensively used for breast cancer detection in different types of breast cancer images such as ultrasound (US), magnetic resonance imaging (MRI), and X-ray as follows:

US Images: Eroğlu Y [11] proposed a hybrid-based CNN system based on ultrasonography images for diagnosing BC by extracting features from Alexnet, MobilenetV2, and Resnet50 then, after concatenating them, mRMR features selection method were used to select the best features. This system used machine learning algorithms support vector machine (SVM) and k-nearest neighbors (k-NN) as a classifier. As a result, an accuracy rate of 95.6% was achieved. Reference [12] An image segmentation method is applied to split the breast US images into sub-regions, followed by an object recognition method that employs feature extraction, selection, and classification techniques to automatically detect the sub-regions related to BC. In [13] a method was suggested to segment BCs via semantic classification and patch merging. The approach involves cropping a region of interest, enhancing it using filters and clustering techniques, extracting features, and performing classification with a neural network and a k-NN classifier.

MRI Images: Zhou J et al. [14] proposed a 3D deep CNN for the detection and localization of BC in dynamic contrast-enhanced MRI data using a weakly supervised approach and achieved 83.7% accuracy. In [15], a multi-layer CNN was designed to classify MRI images as malignant or benign tumors using pixel information and online data augmentation. The network achieved high accuracy as 98.33%.

X-ray Images: Authors in [16] used pre-trained CNN models, InceptionV3 and ResNet50, on the DDSM dataset to differentiate benign and malignant mammogram tumors. Transfer learning, pre-processing, and data augmentation techniques were used due to limited data. ResNet50 achieved 85.7%, and InceptionV3 achieved 79.6% accuracies. In [17], authors used a CNN model that combines features from multiple views of mediolateral oblique (MLO) and craniocaudal (CC). Multi-scale features and a penalty term were used and achieved 82.02% accuracy on the DDSM dataset. Ridhi Hela et al. in [18] proposed a methodology for BC detection using the CBIS-DDSM image dataset. Image pre-processing was done, followed by feature extraction using multiple CNN models (AlexNet, VGG16, ResNet, GoogLeNet, and InceptionResNet). The extracted features were evaluated using a neural network classifier, achieving an accuracy of 88%.

This paper provides two significant contributions to the existing literature. Firstly, it extracts a comprehensive set of features from diverse pre-trained convolutional neural networks (CNNs) for different perspectives. Additionally, it incorporates additional features like age to create a feature vector. Secondly, it employs a methodology to reduce feature vector dimensionality by eliminating weak features based on their mutual information with image labels.

The proposed system uses five base models, namely Alexnet, Resnet50, MobileNetSmall, ConvNeXtSmall, and EfficienNet, whose features are concatenated and extracted for optimal classification with a neural network (NN) model. This approach demonstrated its capability to enhance the accuracy of BC classification.

The rest of the paper is structured as follows: Section 2 outlines the materials and models employed in the study, while Section 3 presents the proposed model. Section 4 discusses the results obtained for various datasets. The paper is concluded in Section 5.

2. Materials and Methods

2.1. Datasets

A. The main dataset for this project is RSNA Screening Mammography BC from a recent Kaggle competition [19]. The dataset contains 54713 images in dicom format, from roughly 11,000 patients. For each patient, there are at least four images from different laterality and views. For each subject, two different views CC and MLO, and images from left and right laterality were provided. The images are of various sizes and formats including jpeg and jpeg 2000 and different types such as monochrome-1 and monochrome-2. The dataset provides additional features which some of them can be used for classification purposes: age, implant, BIRADS, and density. We based our work on this dataset, but since this dataset is new, it has not been used in any published research yet. Hence, for comparison purposes, we used two other well-known datasets MIAS and DDSM. This dataset was imbalanced as only 2 percent of the images were from cancer patients, which makes any

classification method biased. To compensate for this, we used all positive images and only 2320 images from negative cases. Figure 1 depicts two sample images from this dataset for cancer and normal cases.

B. The Mammographic Image Analysis Society (MIAS) [20] dataset is a well-known and widely used dataset for the development and evaluation of CAD systems for BC detection. It consists of 322 mammographic images, with each image accompanied by a corresponding ground truth classification of benign or malignant tumors. The dataset is particularly valuable for researchers interested in developing machine learning algorithms for BC detection, as it includes examples of both normal and abnormal mammograms, as well as a range of breast densities and lesion types. Figure 2 depicts two sample images from this dataset for cancer and normal cases.

C. The Digital Database for Screening Mammography (DDSM) [21] includes 55,890 images, of which 14% are positive, and the remaining 86% are negative. Images were tiled into 598x598 tiles, which were then resized to 299x299. A subset of this dataset which is for positive cases and is called CBIS-DDSM, has been annotated and the region of interest has been extracted by experts. In this research, we do not use the CBIS-DDSM and use the original DDSM dataset as we are classifying the images from normal subjects and cancer patients. Figure 3 depicts two sample images from this dataset for cancer and normal cases.

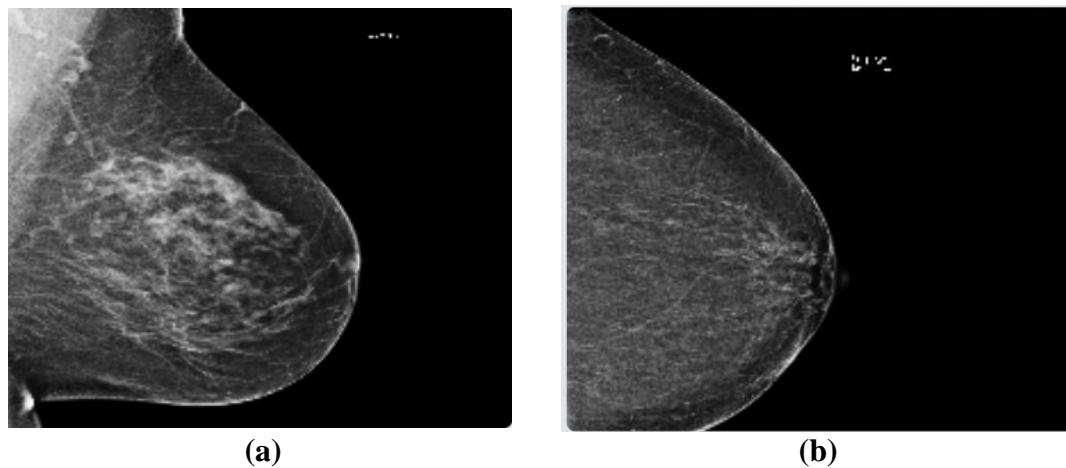


Figure 1. These figures show two sample images from the RSNA dataset for (a) a cancerous, and (b) a normal subject.

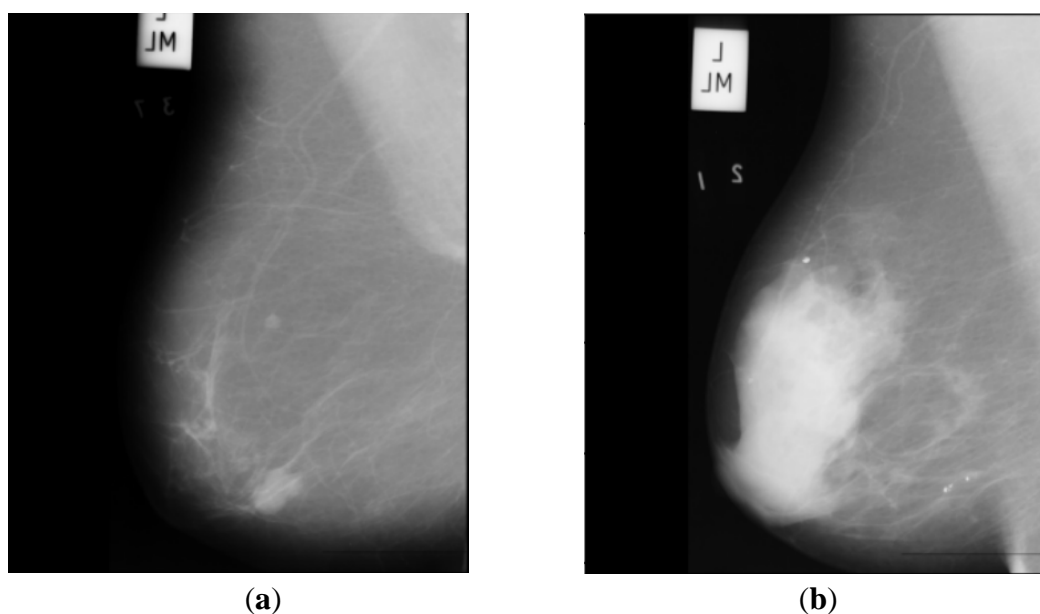


Figure 2. These figures show two sample images from the MIAS dataset for a) cancerous, and b) normal subjects.

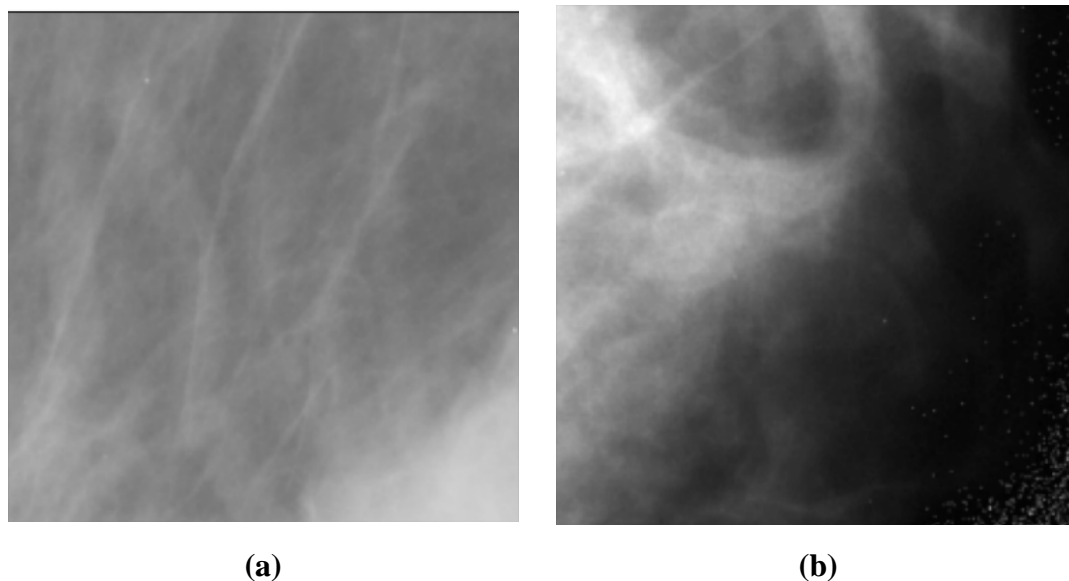


Figure 3. These figures show two sample images from the DDSM dataset for (a) cancerous, and (b) normal subjects.

2.2. Models

A. AlexNet [22] is a deep CNN architecture that was introduced in 2012 and achieved a breakthrough in computer vision tasks such as image classification. It consists of eight layers, including five convolutional layers and three fully connected layers. The first convolutional layer uses a large receptive field to capture low-level features such as edges and textures, while subsequent layers use smaller receptive fields to capture increasingly complex and abstract features. AlexNet was the first deep network to successfully use Rectified Linear Unit (ReLU) activation functions, which have since become a standard activation function in deep learning. It also used dropout regularization to prevent overfitting during training. AlexNet's success on the ImageNet dataset, which contains over one million images, demonstrated the potential of deep neural networks for image recognition tasks and paved the way for further advances in the field of computer vision.

B. ResNet50 [23] is a deep CNN architecture that uses residual connections to enable learning from very deep architectures without suffering from the vanishing gradient problem. It consists of 50 layers, including convolutional layers, batch normalization layers, ReLU activation functions, and fully connected layers. ResNet50 also uses a skip connection that bypasses several layers in the network, allowing it to effectively learn both low-level and high-level features.

C. EfficientNet [24] is a family of deep CNN architectures that were introduced in 2019 and have achieved state-of-the-art performance on a range of computer vision tasks. EfficientNet uses a compound scaling method to simultaneously optimize the depth, width, and resolution of the network, allowing it to achieve high accuracy while maintaining computational efficiency. EfficientNet consists of a backbone network that extracts features from input images and a head network that performs the final classification. The backbone network uses a combination of mobile inverted bottleneck convolutional layers and squeeze-and-excitation (SE) blocks to capture both spatial and channel-wise correlations in the input. The head network uses a combination of global average pooling and fully connected layers to perform the final classification.

D. MobileNet [25] is a deep learning architecture suitable for efficient and accurate analysis of medical images, specifically in the context of BC diagnosis. With its emphasis on computational efficiency, MobileNet can effectively extract features from mammography images, enabling the detection of subtle patterns or abnormalities associated with breast cancer. By utilizing depthwise separable convolutions, MobileNet optimizes memory consumption and computational load, making it ideal for resource-constrained environments. The integration of the ReLU6 activation function further enhances efficiency and compatibility with medical imaging devices. Overall,

MobileNet offers a valuable solution for BC analysis, providing accurate results while operating efficiently on limited computational resources.

E. ConvNeXt [26] is an architecture that enhances the representational capacity of CNNs by leveraging parallel branches to capture diverse and complementary features, leading to improved performance on challenging visual recognition tasks. It has demonstrated excellent performance on various computer vision tasks, including image classification, object detection, and semantic segmentation. Its ability to capture complex relationships between features has made it a popular choice for tasks requiring a high-level understanding of visual data.

3. Proposed Method

In this paper, we propose a method based on extraction and concatenation of features obtained from various CNN models. The extracted features are then reduced such that only good features are selected and then used for the classification of normal and cancerous images. Figure 4 illustrates the block diagram of the proposed system.

A. Feature extraction: For feature extraction, we exploit the features computed by pre-trained CNN models described in Section 2.2. For each model, the features are extracted from the last layer before the last fully connected (FC) layer as the output of the final FC layer has been trained for 1000 classes of the ImageNet dataset and hence, we skip this layer and extract the features from the last layer before the final FC layer. Table 1 depicts the layer before the final FC layer and the number of features extracted for each CNN model used in this paper.

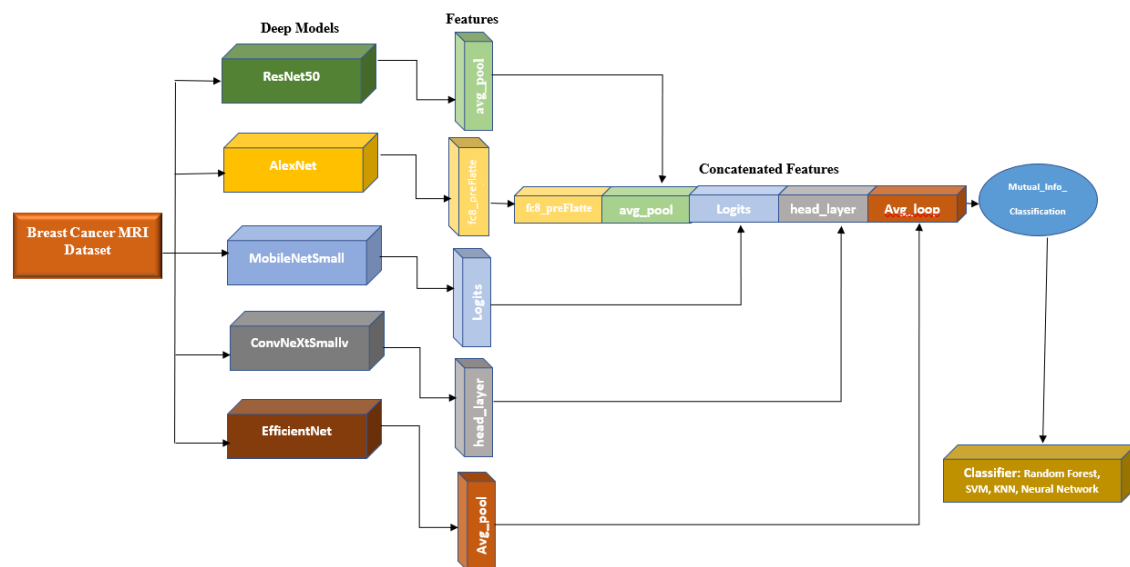


Figure 4. Block diagram of the proposed system.

Table 1. This table shows the CNN models used in the proposed method along with the layer name where the features have been extracted and the number of features extracted from each model.

CNN Models	Layer Name ¹	Number of features
ResNet50	avg_pool	2048
AlexNet	fc8_preFlatten	4096
MobileNetSmall	Logits	1000
ConvNeXtSmall	head_layer	768
EfficientNet	avg_pool	1280

¹ Layer's names have been taken from TensorFlow models.

- B. Feature concatenation: The 1-dimensional (1D) features extracted in the previous step are concatenated to form a single 1D feature vector. Note that for each CNN model, we have extracted features from two different views CC and MLO. Hence, 10 1D vectors are concatenated here. This forms a vector with a size of 18384 For the RSNA dataset that we used as the basis of our research, we have an additional useful feature for the patient age. We can also simply normalize and add age to our feature vector to have 18385 features in total.
- C. Feature selection: The majority of the features are redundant and do not carry any useful information and only increase the complexity of the system. Figure 5 illustrates 2 samples of good and weak features. As one can see from the figure, in the case of weak features, the distribution of the feature for normal and cancerous subjects are similar showing that there is no useful information in this feature and the calculated mutual information between them is zero. For the case of good features, normal and cancerous subjects have obviously different distributions showing that these features carry useful information, although small, that can improve the performance of classifiers used in the next step. In our proposed method, we reduced the number of features by only selecting good features. We define good features as the ones that have mutual information larger than a threshold. To compute mutual information we used the method in [27]. We empirically found a 0.02 threshold gives us the best results. Note that we also adopted feature selection based on mutual information empirically and after using various feature selection methods. The number of features for each dataset before and after feature selection is presented in the below table.
- D. Feature classification: After selecting the best features, we need to classify them. For this purpose, we tried multiple machine learning algorithms such as random forest, SVM, and neural networks. For classification with random forest, we used 100 trees, and for the neural network classifier, we used two fully-connected (FC) layers with 96 and 1 neurons, respectively. For the last FC layer, we used a sigmoid activation function that classifies normal cases from cancerous ones.

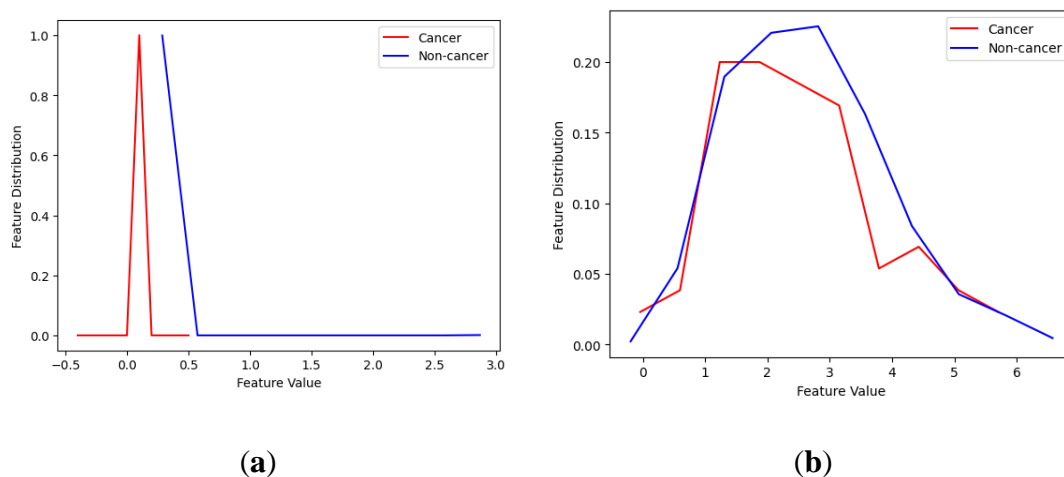


Figure 5. These figures show distributions of (a) a good feature and (b) a weak feature extracted using a pre-trained CNN model. for cancer and noncancer subjects in the DDSM dataset. The mutual information computed for these two features is 0.035 and zero, respectively.

Table 2. The total number of features obtained from each dataset before and after feature selection.

Dataset	Before feature selection	After feature selection
RSNA	18385 ¹	452
MIAS	9192	212
DDSM	9192	206

¹ RSNA dataset provides two views for each subject and one additional feature for age.

4. Results and Discussion

This section presents the results obtained from the three datasets introduced in section 2.1 for models in section 2.2 and a combination of all of them as in Figure 4.

4.1. Evaluation Metrics [28]

To assess the performance of our experiments, we utilized various evaluation metrics.

- True positives (TP): Instances where the predicted class and actual class are both positive. This indicates that the classifier accurately classified the instance with a positive label.
- False positives (FP): Instances where the predicted class is positive but the actual class is negative. This means that the classifier incorrectly classified the instance with a positive label. In the context of breast abnormality classification, an FP response corresponds to a type I error according to statisticians. For example, it could refer to a calcification image being classified as a mass lesion or a benign mass lesion being classified as a malignant mammogram in the diagnosis.
- True negatives (TN): Instances where the predicted class and actual class are both negative. This indicates that the classifier correctly classified the instance with a negative label.
- False negatives (FN): Instances where the predicted class is negative but the actual class is positive. This means that the classifier incorrectly classified the instance with a negative label. In the context of breast abnormality classification, an FN response is considered a type II error. For instance, it could refer to a mass mammogram being classified as calcification or a malignant mass lesion being classified as a benign mammogram in the diagnosis. Type II errors are particularly significant in their consequences .
- Accuracy: This metric represents the overall number of correctly classified instances. In the case of the abnormality classifier, accuracy signifies the correct classification of image patches containing either mass or calcification. Similarly, accuracy shows the correct classification of image patches as either malignant or benign in the pathology classifier.

$$Acc = \frac{(TP+TN)}{(TP+TN+FP+FN)} \quad (1)$$

- Sensitivity or Recall: This metric represents the proportion of positive image patches that are correctly classified. In the abnormality type classifier, sensitivity indicates the fraction of image patches that are truly mass lesions and are correctly classified. Similarly, in the abnormality pathology classifier, it shows the fraction of truly malignant image patches that are correctly classified. Given the significance of type II error, this metric is valuable for evaluating performance.

$$Sn = \frac{TP}{(TP+FN)} \quad (2)$$

- Precision: This metric reflects the proportion of positive predictions that are correctly categorized. It is calculated using the following formula:

$$Pr = \frac{TP}{(TP+FP)} \quad (3)$$

- F1 Score: This measure combines the impact of recall and precision using the harmonic mean, giving equal penalties to extreme values. It is commonly calculated using the formula:

$$F - Score = \frac{(2*Sn*Pr)}{(Sn+Pr)} \quad (4)$$

4.2. Performance Evaluation of the Proposed Model for Different Classifiers

Table 3 presents a comparison of performance metrics for different CNN models using the RSNA dataset. Among the individual CNN models, EfficientNet consistently outperforms the other models in terms of accuracy, sensitivity, precision, AUC, and F-Score. Its superior performance can be attributed to its architecture, which enables it to capture relevant features and make accurate predictions on the RSNA dataset. EfficientNet proves to be the most effective choice among the individual models for accurately classifying medical images in the RSNA dataset. From the last row of the table, one can see that the proposed concatenation scheme, significantly improves all performance metrics, for instance, the achieved accuracy is 6 percent more than the best CNN model, i.e., EfficientNet.

Table 4 presents a summary of the results obtained using the kNN classifier with k=5. The findings indicate a significant decline in performance compared to the NN model. Specifically, without feature concatenation, the highest accuracy is achieved with AlexNet, which is 8 percent lower than the accuracy of the same model with the NN classifier, and 13 percent lower than the best-performing EfficientNet model with the NN classifier. Additionally, the accuracy of the concatenated model is also 14 percent lower compared to the concatenated model with the NN classifier.

Table 5 displays the results obtained from the random forest classifier. It demonstrates that the accuracy of the concatenated Model is equivalent to that of the KNN classifier, but falls short compared to the neural network. Among the individual models, EfficientNet exhibits the most favorable performance metrics, while mobileNetSmall exhibits the least favorable performance.

Table 6 displays the results of the proposed method using the SVM classifier. It is evident from the table that SVM exhibits the lowest accuracy among all four investigated methods. Specifically, the accuracy of the SVM-based method is 19 percent lower than that of the NN-based method. Furthermore, in comparison to the KNN and RandomForest-based systems, the accuracy of the concatenated model decreased by 5 percent.

Table 3. Performance comparison of the proposed method for different CNN models and Concat. Model with the NN classifier for RSNA dataset.

CNN Models	Acc	Sn	Pr	AUC	F-Score
AlexNet	81%	84%	87%	0.82	0.86
Resnet50	84%	90%	86%	0.89	0.88
MobileNetSmall	77%	85%	81%	0.81	0.83
ConvNexSmall	79%	87%	83%	0.83	0.85
EfficientNet	86%	92%	88%	0.92	0.90
Concat. Model	92%	96%	92%	0.96	0.94

Table 4. Performance comparison of the proposed method for different CNN models and Concat. Model with the kNN classifier for RSNA dataset.

CNN Models	Acc	Sn	Pr	AUC	F-Score
AlexNet	73%	70%	72%	0.70	0.71
Resnet50	72%	75%	71%	0.73	0.73
MobileNetSmall	64%	71%	67%	0.68	0.69
ConvNexSmall	66%	74%	70%	0.71	0.72
EfficientNet	71%	78%	74%	0.76	0.76
Concat. Model	78%	81%	79%	0.82	0.80

Table 5. Performance comparison of the proposed method for different CNN models and Concat. Model with the Random Forest classifier for RSNA dataset.

CNN Models	Acc	Sn	Pr	AUC	F-Score
AlexNet	71%	67%	69%	0.68	0.68
Resnet50	69%	70%	67%	0.71	0.68
MobileNetSmall	60%	67%	63%	0.64	0.65
ConvNexSmall	62%	69%	65%	0.67	0.67
EfficientNet	73%	74%	70%	0.75	0.72
Concat. Model	78%	79%	77%	0.80	0.78

Table 6. Performance comparison of the proposed method for different CNN models and Concat. Model with the SVM classifier for RSNA dataset.

CNN Models	Acc	Sn	Pr	AUC	F-Score
AlexNet	62%	61%	63%	0.62	0.62
Resnet50	64%	66%	63%	0.65	0.64
MobileNetSmall	60%	63%	59%	0.60	0.61
ConvNexSmall	62%	65%	61%	0.63	0.63
EfficientNet	68%	70%	66%	0.68	0.68
Concat. Model	73%	75%	72%	0.74	0.73

4.3. Comparison of the Proposed System with State-of-the-art Methods

Based on the findings presented in Tables 3-6, it is evident that the neural network (NN) classifier achieves the highest level of performance. Therefore, we employ the suggested approach using the NN classifier as the benchmark to compare it with the existing methods.

To the best of our knowledge, the RSNA dataset has not been utilized in any previously published papers. Consequently, for the purposes of this section, we conducted a comparison of our proposed model against existing methods using the MIAS and DDSM datasets and summarized the results in Table 7.

Upon examining Table 7, it is evident that our proposed model has exhibited superior performance compared to state-of-the-art algorithms in terms of accuracy and sensitivity across both the MIAS and DDSM datasets. While the method described in [29] demonstrated slightly better precision for the MIAS dataset, our algorithm outperformed it in the remaining two performance metrics.

Table 7. Performance comparison of our proposed model against vs. methods using the MIAS and DDSM datasets.

Method	Dataset	Number Of Images	ACC	Sn	Pr
SVM & Hough[29]	MIAS & InBreast	322&206	86.13%	80.67%	92.81%
LQP & SVM [30]	MIAS	95	94%	NA	NA
GMM & SVM [31]	Mini-MIAS dataset	90	92.5%	NA	NA
KNN [32]	Mini-MIAS	120	92%	NA	NA
Voting Classifier[33]	MIAS	322	85%	NA	NA
CNN-4d [34]	Mini-MIAS	547	89.05%	90.63%	83.67%
CNN [35]	DDSM	10,480	93.5%	NA	NA
CNNs [36]	DDSM	11,218	85.82%	82.28%	86.59%
Our Method+NN	MIAS	322	94.5%	96.32%	91.80%
Our Method+NN	DDSM	55,890	96%	94.70%	97%

5. Conclusions

We proposed a novel method for accurately diagnosing breast cancer in mammography images. By extracting and selecting features from multiple pre-trained convolutional neural network models, and then classifying them using various machine learning algorithms, we achieved impressive results for different datasets. We showed that the proposed scheme obtains its best performance with a neural network-based classifier. Accuracies as high as 92%, 94.5%, and 96% were achieved for RSNA, MIAS, and DDSM datasets, respectively. Comparisons with existing methods showcased the superiority of our approach, particularly in terms of accuracy and sensitivity. These outcomes highlight the potential of our method to significantly improve the prognosis of breast cancer through timely and precise diagnosis.

Author Contributions: Z.J. provided, and cleaned the dataset, and implemented the algorithms, and Z.J and E.K. performed experiments and wrote the paper. E.K. edited the paper.

Data Availability Statement: Not applicable.

Acknowledgments: We would like to thank Morteza Golzan and Hamideh Mehri for their support.

Conflicts of Interest: The authors declare no conflict of interest.

References

1. Ferlay J, Colombet M, Soerjomataram I, Parkin DM, Piñeros M, Znaor A, Bray F. Cancer statistics for the year 2020: An overview. *International journal of cancer*. 2021 Aug 15;149(4):778-89.
2. Lei S, Zheng R, Zhang S, Wang S, Chen R, Sun K, Zeng H, Zhou J, Wei W. Global patterns of breast cancer incidence and mortality: A population-based cancer registry data analysis from 2000 to 2020. *Cancer Communications*. 2021 Nov;41(11):1183-94.
3. Marks JS, Lee NC, Lawson HW, Henson R, Bobo JK, Kaeser MK. Implementing recommendations for the early detection of breast and cervical cancer among low-income women. *Morbidity and Mortality Weekly Report: Recommendations and Reports*. 2000 Mar 31:35-55.
4. Du-Crow E. *Computer-Aided Detection in Mammography*. The University of Manchester (United Kingdom); 2022.
5. Evans A, Trimboli RM, Athanasiou A, Balleyguier C, Baltzer PA, Bick U, Camps Herrero J, Clauser P, Colin C, Cornford E, Fallenberg EM. Breast ultrasound: recommendations for information to women and referring physicians by the European Society of Breast Imaging. *Insights into imaging*. 2018 Aug;9:449-61.
6. Schueller G, Schueller-Weidekamm C, Helbich TH. Accuracy of ultrasound-guided, large-core needle breast biopsy. *European radiology*. 2008 Sep;18:1761-73.

7. Agarwal S, Yadav AS, Dinesh V, Vatsav KS, Prakash KS, Jaiswal S. By artificial intelligence algorithms and machine learning models to diagnosis cancer. *Materials Today: Proceedings*. 2021 Jul 24.
8. Bai J, Posner R, Wang T, Yang C, Nabavi S. Applying deep learning in digital breast tomosynthesis for automatic breast cancer detection: A review. *Medical image analysis*. 2021 Jul 1;71:102049.
9. Li Z, Liu F, Yang W, Peng S, Zhou J. A survey of convolutional neural networks: analysis, applications, and prospects. *IEEE Transactions on neural networks and learning systems*. 2021 Jun 10.
10. Zuluaga-Gomez J, Al Masry Z, Benaggoune K, Meraghni S, Zerhouni N. A CNN-based methodology for breast cancer diagnosis using thermal images. *Computer Methods in Biomechanics and Biomedical Engineering: Imaging & Visualization*. 2021 Mar 4;9(2):131-45.
11. Eroğlu Y, Yildirim M, Çinar A. Convolutional Neural Networks based classification of breast ultrasonography images by hybrid method with respect to benign, malignant, and normal using mRMR. *Computers in biology and medicine*. 2021 Jun 1;133:104407.
12. Huang Q, Yang F, Liu L, Li X. Automatic segmentation of breast lesions for interaction in ultrasonic computer-aided diagnosis. *Information Sciences*. 2015 Sep 1;314:293-310.
13. Huang Q, Huang Y, Luo Y, Yuan F, Li X. Segmentation of breast ultrasound image with semantic classification of superpixels. *Medical Image Analysis*. 2020 Apr 1;61:101657.
14. Zhou J, Luo LY, Dou Q, Chen H, Chen C, Li GJ, Jiang ZF, Heng PA. Weakly supervised 3D deep learning for breast cancer classification and localization of the lesions in MR images. *Journal of Magnetic Resonance Imaging*. 2019 Oct;50(4):1144-51.
15. Yurttakal AH, Erbay H, İkizceli T, Karaçavuş S. Detection of breast cancer via deep convolution neural networks using MRI images. *Multimedia Tools and Applications*. 2020 Jun;79:15555-73.
16. Rahman AS, Belhaouari SB, Bouzerdoum A, Baali H, Alam T, Eldaraa AM. Breast mass tumor classification using deep learning. In *2020 IEEE International Conference on Informatics, IoT, and Enabling Technologies (ICIoT) 2020 Feb 2 (pp. 271-276)*. IEEE.
17. Sun L, Wang J, Hu Z, Xu Y, Cui Z. Multi-view convolutional neural networks for mammographic image classification. *IEEE Access*. 2019 Sep 3;7:126273-82.
18. Heravi EJ, Aghdam HH, Puig D. Classification of Foods Using Spatial Pyramid Convolutional Neural Network. In *CCIA 2016 Sep 21 (pp. 163-168)*.
19. Carr C., Kitamura F., Partridge G., Kalpathy-Cramer J., Mongan J., Andriole K., Lavender, Vazirabad M., Riopel M., Ball R., Dane S., Chen Y. *RSNA Screening Mammography Breast Cancer Detection, Kaggle 2022*, URL <https://kaggle.com/competitions/rsna-breast-cancer-detection>.
20. Suckling J, Parker J, Dance D, Astley S, Hutt I, Boggis C, Ricketts I, Stamatakis E, Cerneaz N, Kok S, Taylor P. *Mammographic image analysis society (mias) database v1*. 21.
21. Heath M, Bowyer K, Kopans D, Kegelmeyer P, Moore R, Chang K, Munishkumaran S. Current status of the digital database for screening mammography. *Digital Mammography: Nijmegen, 1998*. 1998:457-60.
22. Krizhevsky A, Sutskever I, Hinton GE. Imagenet classification with deep convolutional neural networks. *Communications of the ACM*. 2017 May 24;60(6):84-90.
23. He K, Zhang X, Ren S, Sun J. Deep residual learning for image recognition. In *Proceedings of the IEEE Conference on computer vision and pattern recognition 2016 (pp. 770-778)*.
24. Tan M, Le Q. Efficientnetv2: Smaller models and faster training. *International conference on machine learning 2021 Jul 1 (pp. 10096-10106)*. PMLR.

25. Howard AG, Zhu M, Chen B, Kalenichenko D, Wang W, Weyand T, Andreetto M, Adam H. Mobilenets: Efficient convolutional neural networks for mobile vision applications. arXiv preprint arXiv:1704.04861. 2017 Apr 17.
26. Liu Z, Mao H, Wu CY, Feichtenhofer C, Darrell T, Xie S. A convnet for the 2020s. In Proceedings of the IEEE/CVF Conference on Computer Vision and Pattern Recognition 2022 (pp. 11976-11986).
27. Ross BC. Mutual information between discrete and continuous data sets. PloS one. 2014 Feb 19;9(2):e87357.
28. Azour F, Boukerche A. An efficient transfer and ensemble learning-based computer-aided breast abnormality diagnosis system. IEEE Access. 2022 Jul 25.
29. Rampun A, Scotney BW, Morrow PJ, Wang H, Winder J. Breast density classification using local quinary patterns with various neighbourhood topologies. Journal of Imaging. 2018 Jan 8.
30. Vijayarajeswari R, Parthasarathy P, Vivekanandan S, Basha AA. Classification of mammogram for early detection of breast cancer using SVM classifier and Hough transform. Measurement. 2019 Nov 1;146:800-5.
31. Arafa AA, El-Sokary N, Asad A, Hefny H. Computer-aided detection system for breast cancer based on GMM and SVM. Arab Journal of Nuclear Sciences and Applications. 2019 Apr 1;52(2):142-50.
32. Diaz RA, Swandewi NN, Novianti KD. Malignancy determination breast cancer based on mammogram image with k-nearest neighbor. In 2019 1st International Conference on Cybernetics and Intelligent System (ICORIS) 2019 Aug 22 (Vol. 1, pp. 233-237). IEEE.
33. Agrawal S, Rangnekar R, Gala D, Paul S, Kalbande D. Detection of breast cancer from mammograms using a hybrid approach of deep learning and linear classification. In 2018 International Conference on Smart City and Emerging Technology (ICSCET) 2018 Jan 5 (pp. 1-6). IEEE.
34. Li B, Ge Y, Zhao Y, Guan E, Yan W. Benign and malignant mammographic image classification based on convolutional neural networks. In Proceedings of the 2018 10th International Conference on Machine Learning and Computing 2018 Feb 26 (pp. 247-251).
35. Platania R, Shams S, Yang S, Zhang J, Lee K, Park SJ. Automated breast cancer diagnosis using deep learning and region of interest detection (bc-droid). In Proceedings of the 8th ACM international conference on bioinformatics, computational biology, and health informatics 2017 Aug 20 (pp. 536-543).
36. Swiderski B, Kurek J, Osowski S, Kruk M, Barhoumi W. Deep learning and non-negative matrix factorization in recognition of mammograms. In Eighth International Conference on Graphic and Image Processing (ICGIP 2016) 2017 Feb 8 (Vol. 10225, pp. 53-59). SPIE.

Disclaimer/Publisher's Note: The statements, opinions and data contained in all publications are solely those of the individual author(s) and contributor(s) and not of MDPI and/or the editor(s). MDPI and/or the editor(s) disclaim responsibility for any injury to people or property resulting from any ideas, methods, instructions or products referred to in the content.